

Determining reactor fuel type from continuous antineutrino monitoring

Patrick Jaffke^{1,*} and Patrick Huber¹

¹*Center for Neutrino Physics, Virginia Tech, Blacksburg, VA, USA*

(Dated: November 15, 2021)

We investigate the ability of an antineutrino detector to determine the fuel type of a reactor. A hypothetical 5 t antineutrino detector is placed 25 m from the core and measures the spectral shape and rate of antineutrinos emitted by fission fragments in the core for a number of 90 d periods. Our results indicate that four major fuel types can be differentiated from the variation of fission fractions over the irradiation time with a true positive probability of detection at $\sim 95\%$. In addition, we demonstrate that antineutrinos can identify the burn-up at which weapons-grade mixed-oxide (MOX) fuel would be reduced to reactor-grade MOX on average, providing assurance that plutonium disposition goals are met. In addition, we investigate removal scenarios where plutonium is purposefully diverted from a mixture of MOX and low-enriched uranium (LEU) fuel. Finally, we discuss how our analysis is impacted by a spectral distortion around 6 MeV observed in the antineutrino spectrum measured from commercial power reactors.

The end of the Cold War after the collapse of the Soviet Union in 1991 left the United States and Russia with a large number of surplus nuclear weapons [1]. Ultimately, the plutonium contained in these surplus nuclear weapons needs to be disposed of. There are various techniques proposed for the disposal of weapons plutonium, see for instance Ref. [2], and one of these techniques is based on so-called mixed oxide fuel (MOX), where a large part of the fissile content in regular reactor fuel is replaced with the to-be-disposed plutonium. This MOX fuel can be used in commercial light-water reactors and would thus allow one to convert some of the plutonium to usable energy. The remaining plutonium which is not fissioned will undergo a major change of its isotopic composition rendering it less attractive for the use in nuclear weapons. Moreover, whatever is left will be embedded in highly radioactive spent reactor fuel, making retrieval expensive and difficult. MOX fuel is successfully employed in Europe, in particular in France a significant number of power plants are using MOX fuel on an ongoing basis. In the MOX approach to plutonium disposal, the primary quantitative measure of reaching the disposition goal is given by burn-up: fuel which has reached a certain burn-up threshold will both have a significantly changed mix of plutonium isotopes as well as be sufficiently protected by its own radiation field. In this paper we investigate how continuous antineutrino monitoring can be used as a complementary verification technique of both disposal goals by directly measuring the burn-up and ratio of plutonium-239 to plutonium-241, which serves as a proxy for the fraction of plutonium-240; plutonium-240 is not fissile and thus does not have its own, direct neutrino signature. In addition, we study the hypothetical scenario of the intentional removal of plutonium.

The monitoring of nuclear reactors via antineutrino emission was first postulated nearly 40 years ago by Borovoi and Mikaelyan [3]. This concept has seen a recent resurgence as a safeguards or verification tech-

nique [4–9], where antineutrinos offer the unique advantages of independence of operation declarations and the ability to recover from a loss of continuity [10]. This type of reactor monitoring would require surface-level detector technology, which has yet to be demonstrated with sufficient fidelity but is the current goal of many short-baseline neutrino experiments [11].

Antineutrino monitoring relies on the fact that fissions of different fissile nuclides, such as $^{235,238}\text{U}$ or $^{239,241}\text{Pu}$, produce different spectral shapes in antineutrino energy. An overall measurement of the rate of antineutrinos will determine the power of the reactor, while a spectral decomposition can infer the core content. These techniques were employed previously [6, 10] to study the capabilities of antineutrinos based on real-world scenarios. We use the same process in this work.

Typically, the fuel evolution of the reactor of interest is simulated, and thus the fission rates throughout the irradiation cycle are obtained. This allows one to compute the total antineutrino spectrum by weighting these fission rates with the appropriate antineutrino yields from a single fission of each fissioning isotope. The uncertainties in these yields can be reduced with a previous calibration of the antineutrino detector to a core with known composition and we assume this calibration has been performed. The total antineutrino signal represents the ‘observed’ spectrum in our simulated experiment. The expected events are separated into energy bins to acquire the spectral shape, represented by

$$n_i = N \int_{E_i - \Delta E/2}^{E_i + \Delta E/2} \sigma(E) \vec{F} \cdot \vec{S}(E) dE, \quad (1)$$

with the width of the energy bin ΔE , the interaction cross-section $\sigma(E)$ [12], the fission rate vector \vec{F} , and the vector of antineutrino yields from each fissile $\vec{S}(E)$ [13, 14]. The normalization N takes into ac-

count the detector size, location¹, and overall efficiency. The choice of ΔE must be small enough to allow for good resolution in the spectral shape. We have chosen $\Delta E = 250$ keV and a detection threshold of 2 MeV. Previous large-scale experiments have demonstrated the ability to reach this level of energy resolution [15–17] and future short-baseline detectors are aiming to match or exceed this, see for instance Ref. [18].

One can compute a log-likelihood ratio by comparing the observed spectrum, created by weighting the simulated fission rate vector \vec{F}_S with the fluxes $\vec{S}(E)$, to the expected spectral shape of Eq. 1. Minimizing the resulting χ^2 -function, given below

$$\chi^2(\vec{F}) = \sum_i^N \frac{(n_i(\vec{F}) - n'_i)^2}{n'_i}, \quad (2)$$

provides the best-fit fission rate vector \vec{F} (or maximum likelihood estimate), where the observed events from \vec{F}_S in bin i are n'_i . This measurement of the fission rate vector is then used to determine the core type and progression along its irradiation cycle. Detection statistics are simulated by randomizing the n'_i with a Poisson distribution. We assume detection statistics dominate the error budget as precise detector calibration and simulation have been achieved below the few percent level and accurate background measurements have been incorporated into previous calibration techniques [19].

The simulated reactor is a Westinghouse-style light water reactor (LWR) loaded with various core compositions. The details of the simulation and the core configuration and characteristics are given in Ref. [20]. Our analysis is primarily concerned with four core types. The first is weapons-grade MOX (WGMOX) used in the LWR, corresponding to the actual disposition case. The second is reactor-grade MOX (RGMOX), which corresponds the plutonium vector of discharged uranium-based fuel, and usually is part of a fuel cycle which includes reprocessing of spent fuel. The third fuel type is a mixture of two-thirds low-enriched uranium (LEU) fuel and one third of WGMOX, where one third corresponds approximately to the MOX fraction used in France². Finally, the fourth core is a full LEU core. Initial fuel compositions are described and provided in Ref. [20] for the various cores considered here. All four cores are simulated to run for a total of 500 d of irradiation at full power, corresponding to a burn-up of 21 MW d/kg HM. Thus, the fission rates from these simulations have an implicit time-dependence $\vec{F}(t)$ and Eq. 1 is modified with an integration over the detection time T . This implies that the observed spec-

tral shape will depend on *when* the detector monitors the reactor.

Two hundred cases were simulated for each of the four core types and four different detection periods. These individual cases represent different Poisson-randomized antineutrino spectra from the simulated fission rates \vec{F}_S . Each case was minimized via Eq. 2 producing a best-fit core-averaged \vec{F} for that detection period and fuel content. One can evaluate the best-fit fission rate vector in various forms, such as the total plutonium fission fraction versus the plutonium-239 fission fraction as in Fig. 1. We can see that within the first 90 d measure-

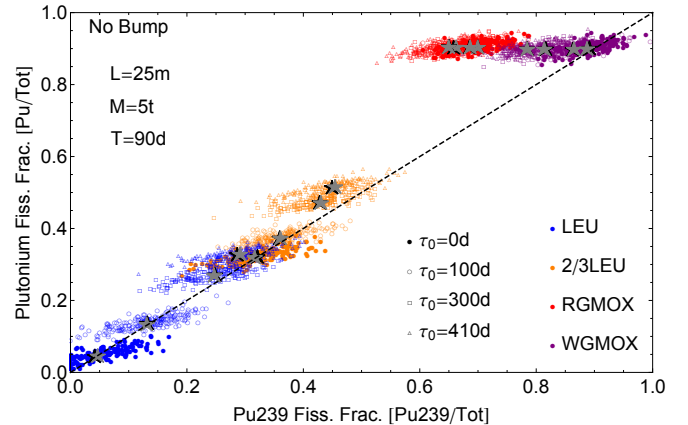


FIG. 1. Plot of the derived best-fit plutonium and plutonium-239 fission fractions for four different fuel inventories and four different detection periods. The progression of fuel is illustrated by the movement of the centroids (stars) for each set. Black centroids are calculated from the data points and the gray are directly from the simulated fission rates. The dashed line is the physically-real plutonium boundary.

ment (i.e. the start time is $\tau_0 = 0$ d) the cores appear as expected. The pure LEU core (blue) contains a majority of uranium fission and very little plutonium. The core with one third WGMOX (orange) contains a sizable amount of plutonium initially and the plutonium is a high-percentage plutonium-239, as the centroid falls near the pure plutonium-239 dashed line. For the MOX cores, the reactor-grade plutonium (red) begins far from the purity line and has mostly plutonium fissions. The WGMOX core (purple) begins on the purity line and also has a majority of plutonium fissions. The black centroids are found by evenly weighting all data points in a particular set, including those that fall in non-physical regimes, such as points beyond the pure plutonium-239 line. The gray centroids mark the time-averaged value of the fission quantity during its irradiation period, directly calculated from the simulated time-dependent fission rates.

From Fig. 1 we note that the initial state of the mixed LEU+WGMOX core looks nearly identical to that of the last detection period of the pure LEU core. This degeneracy can be broken when we consider continuous

¹ We assume a baseline short enough to avoid neutrino oscillations via active neutrinos.

² Obviously, France is using RGMOX.

antineutrino monitoring. With continuous monitoring, one would know the starting irradiation time and relative power from the rate measurement. With multiple measurements of the antineutrino spectrum one could infer core inventory based on the trajectory of two consecutive measurements, say $\tau_0 = 0$ d and $\tau_0 = 100$ d. A trajectory that moves along the pure plutonium-239 line is comprised of mostly LEU. Horizontal shifts are cores that contain mostly MOX. We also note that the antineutrino-derived fission fractions (black stars) are within a few percent of the simulated values (gray stars) in Fig. 1.

To acquire information on the plutonium grade, an important factor in weapons-production [21], one can use a ratio of the plutonium fission rates. We use the ratio of plutonium-239 fission rate to the total plutonium fission rate, which we label as the plutonium fission grade (G_{Pu}). Using $G_{\text{Pu}} = 90\%$ as the disposition goal³, we find based on the antineutrino measurement alone that 16% (31%) of WGMOX (LEU+MOX) cores remained above this goal at the final (410 – 500 d) measurement period. The sensitivity to downgrading the plutonium is worse in the mixed core as the uranium absorbs some of the total fission rates, thus slowing the progression of plutonium fissions from weapons-grade to reactor-grade. In addition, this measurement represents a core-averaged plutonium ratio, so a lower G_{Pu} requirement would be necessary to ensure all assemblies fall below the weapons-barrier or an assembly-by-assembly technique would need to be employed as well [22].

The trajectory and the absolute distance traveled in the fission quantity plane can be calculated from Fig. 1 and compared between different cores and different measurement periods. For example, the LEU cores both travel along the same trajectory, but the pure LEU core has a much larger difference between two adjacent measurement periods than the mixed core. This quantity, which we label the differential burn-up, is given by

$$\Delta \vec{F} = \frac{\vec{F}(t_f) - \vec{F}(t_i)}{\vec{F}(t_f)}, \quad (3)$$

where the fission fraction $\vec{F}(t)$ is created from the best-fit values of the fission rate vector $\vec{F}(t)$. We have computed the differential burn-up between the four measurement periods for each of the four simulated cores in Tab. I. The trends noted above appear quantitatively in this differential burn-up analysis (DBA). For example, both LEU-type cores have a positive ΔF_{Pu} across all time steps, indicating that these cores are producing plutonium. However, the LEU core mixed with WG plutonium has a significantly smaller ΔF_{Pu} indicating that the *rate* of plutonium production in the mixed core is dramatically slower

Differential Burn-up [$\Delta F_{\text{Pu}239}, \Delta F_{\text{Pu}}$] in percent			
	$\tau_0 = 100$ d	$\tau_0 = 300$ d	$\tau_0 = 410$ d
LEU	[218, 201]	[498, 493]	[589, 616]
2/3 LEU	[11.8, 16.1]	[33.2, 46.6]	[39.9, 59.5]
RGMOX	[-2.05, -0.01]	[-5.96, -0.10]	[-7.10, 0.17]
WGMOX	[-3.20, -0.39]	[-8.41, -0.25]	[-12.0, -0.23]
Nominal	[8.40, 14.0]	[30.0, 38.0]	[31.1, 48.9]
8 Rem.	[10.1, 14.6]	[30.3, 40.9]	[40.9, 54.2]
20 Rem.	[20.5, 20.5]	[44.9, 52.1]	[57.4, 68.2]

TABLE I. Differential burn-up analysis (DBA) of the plutonium-239 fission fraction $\Delta F_{\text{Pu}239}$ and the plutonium fission fraction ΔF_{Pu} between the initial $\tau_0 = 0$ d measurement period and the three following measurement periods in percent. The DBA is conducted for the four simulated cores and is given as ordered pairs. Also listed are the DBA results for the removal cases where no fresh WGMOX assemblies (Nominal), 8, or all 20 are replaced with LEU fuel.

by about an order of magnitude for all time steps. In addition, the grade of the plutonium decreases faster for the WGMOX core than the RGMOX core. This difference is much more subtle and develops slowly, but results in an almost doubling of $|\Delta F_{\text{Pu}239}|$, as can be seen in Tab. I.

Another possible scenario is the intentional removal of plutonium from a core, such as the mixed LEU and WGMOX core [20]. The mixed core uses a total of 48 MOX assemblies, 28 of which are once or twice-irradiated and therefore not considered WGMOX any longer. This staggered burning is used in reactor operation to flatten the neutron spectrum distribution. We investigate three scenarios: the first is the nominal run with no removal of the fresh WGMOX assemblies. The second considers removing 8 fresh WGMOX assemblies from the periphery of the reactor and replacing them with LEU assemblies. The fission rate at the edge of the reactor core is relatively low and thus this case will be a particular challenge for antineutrino monitoring. The final case considers a full removal and replacement of all (20) fresh WGMOX assemblies. We plot these scenarios and their exclusion contours in the $F_{\text{Pu}239} - F_{\text{Pu}}$ plane for the initial and final time-step in Fig. 2. For the removal cases, we see that the differential burn-up vectors are all aligned in relatively the same direction, but the magnitudes are slightly different. One can also note that the differences between the removal cases are much less pronounced than those for the full cores, as seen in Tab. I. Furthermore, it becomes apparent that the equilibrium fission rates for each scenario are nearly identical, making this difference more difficult to detect at later irradiation times.

The analyses in Figs. 1, 2, and Tab. I demonstrate the process by which an antineutrino detector would infer the core content of a nuclear reactor. Several time steps are needed to determine the progression of the fuel and

³ The thermal fission cross section of ^{241}Pu is 35% higher than the one of ^{239}Pu , thus in a mixture of 93% ^{239}Pu and 7% ^{241}Pu 90% of all fission will take place in ^{241}Pu .

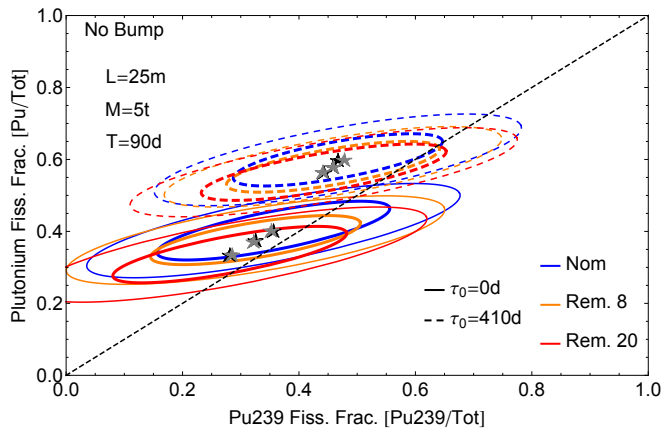


FIG. 2. Plot of the allowed region contours of the best-fit plutonium-239 and total plutonium fission fractions. The contours are derived by fitting Gaussian ellipses to the case distribution. The thick inner ellipse denotes the 1σ quartile and the thin outer ellipse the 2σ quartile. Centroids derived from the ellipses (black) and from the simulated fission rates (gray) are shown. The dashed line is the physically-real plutonium boundary.

identify the differential burn-up. The sign and magnitude resulting from DBA can distinguish between LEU, mixed LEU and MOX, and MOX cores easily, but the difference between RGMOX and WGMOX is more subtle. An absolute measurement of the fission fractions can help to distinguish the latter cases. Next, we present the sensitivity analysis for these absolute measurements.

It is now possible to determine the true and false positive rates (FPR) from the data generated so far. In Fig. 3, we project the data onto the axis represented by the fission fraction of plutonium-239. For each of the histograms we can determine the parameters of a normal distribution, that is the mean and standard deviation. The resulting normal distributions are used to compute the true and false positive rates as a function of the plutonium-239 fission fraction. To allow a simple summary, we chose the critical value in this variable such that the false negative and false positive rates are equal and we will quote this common value. In the language of a receiver operating characteristics, this corresponds to the balance point.

One can determine the false positive rate and the balance point for the four core and measurement period distributions along the various fission fraction axes. First, the simulated experiments are binned along an axis; Fig. 3 provides the projection of Fig. 1 onto its x-axis of plutonium-239 fission fraction. As one would expect from Fig. 3, we observe a very small FPR during the first measurement period ($\sim 0.1\%$ between the LEU cores and $\sim 0.4\%$ between the MOX cores). The second measurement shows more significant FPR of $\sim 1\%$ between both the LEU cores and both the MOX cores. The third measurement begins to show a higher FPR

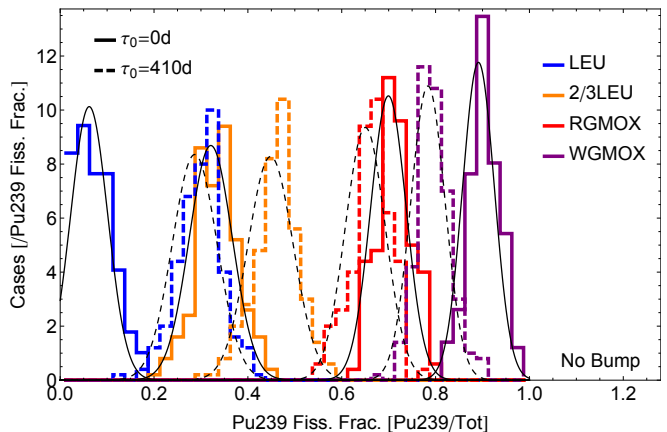


FIG. 3. Histogram of the determined plutonium-239 fission fraction of the simulated cases for the first and last measurement times and four core compositions and the corresponding Gaussian distributions. This represents Fig. 1 projected onto its x-axis.

between the RGMOX and mixed LEU+WGMOX cores, but only around 0.3% . The FPR between the LEU cores is $\sim 3\%$ and between the MOX cores is $\sim 1.8\%$. The last measurement shows a FPR between the LEU cores at 4.6% , between the MOX cores at 4.6% , and between the LEU+WGMOX and RGMOX cores at $\sim 1.3\%$. The information for the first and last measurements is given quantitatively in Tab. II.

The low FPR indicate that only $\sim 5\%$ of cases will be misidentified. Multiple tests with different $\vec{F}(t)$ can isolate and enhance this accuracy. For example, the plutonium or uranium fission fraction has very good separation between the LEU and pure MOX cores, but is completely unable to distinguish between RGMOX and WGMOX. Using the plutonium-239 grade, the FPR drops by about a factor of 3 between the RGMOX and WGMOX cores, but increases drastically for the LEU cores due to the lower plutonium fission fractions. For the removal scenarios, the FPRs are consistently above 50% among all measurements, removal scenarios, and fission fraction tests, implying that detection of those is beyond the capabilities of antineutrino monitoring. This is primarily because antineutrinos measure core-averaged quantities instead of individual assemblies.

Recently, a spectral distortion was observed near 5 MeV (positron energy) in the reactor antineutrino flux of multiple large-statistics experiments [15–17]. The origin of this so-called bump is unknown, but several theories have been explored [23–25]. Irrespective of the bump explanation, one can verify the impact of the spectral feature on the fuel determination by artificially placing the observed bump in the converted antineutrino fluxes.

We choose to place the spectral feature in either uranium-235 or plutonium-239. Using Fig. 2 in Ref. [15], the bump is modeled as a Gaussian distribution where

		False Positive Rates								
		No Bump			U235 Bump			Pu239 Bump		
		LEU+MOX	RGMOX	WGMOX	LEU+MOX	RGMOX	WGMOX	LEU+MOX	RGMOX	WGMOX
First	LEU	0.119%	$< 10^{-4}\%$	$< 10^{-4}\%$	0.00380%	$< 10^{-4}\%$	$< 10^{-4}\%$	$< 10^{-4}\%$	$< 10^{-4}\%$	$< 10^{-4}\%$
	LEU+MOX		$< 10^{-4}\%$	$< 10^{-4}\%$		$< 10^{-4}\%$	$< 10^{-4}\%$		$< 10^{-4}\%$	$< 10^{-4}\%$
	RGMOX			0.377%			0.0318%			$< 10^{-4}\%$
Last	LEU	4.60%	0.00290%	$< 10^{-4}\%$	0.612%	$< 10^{-4}\%$	$< 10^{-4}\%$	$< 10^{-4}\%$	$< 10^{-4}\%$	$< 10^{-4}\%$
	LEU+MOX		1.31%	0.00385%		0.0533%	$< 10^{-4}\%$		$< 10^{-4}\%$	$< 10^{-4}\%$
	RGMOX			4.61%			1.21%			$< 10^{-4}\%$

TABLE II. Upper triangular portion of the core separation FPR matrices using the plutonium-239 fission fraction. Each upper triangular cell corresponds to the percentage of falsely identified cores between the various core compositions. This is done for the three considered locations of the spectral structure (no bump, a uranium-235 bump, and a plutonium-239 bump) and for the first ($\tau_0 = 0$ d) and last ($\tau_0 = 410$ d) measurement periods. The total FPR matrix is symmetric, as expected. A reduction in the FPR by about a factor of 3 occurs between the RGMOX and WGMOX cores when using the plutonium grade as a diagnostic.

the mean and variance are determined by a least-squares fit. We note that the normalization of the Gaussian is fixed by the fission fractions and overall neutrino rate in the relevant bins. The three Gaussian best-fit parameters vary by only a small amount when fixing them instead by Ref. [16] or Ref. [17]. With these new artificial fluxes, we repeat the process outlined above and generate more sample simulations. As expected, a new spectral distortion in either uranium-235 or plutonium-239 enhances the abilities of an antineutrino detector to distinguish between fuel types. A bump in uranium-235 has the effect of pinching the spread of F_{Pu} in Fig. 1 as the uranium-235 fission rate, now easily determined by the spectral distortion, essentially fixes the total plutonium fissions. A bump in plutonium-239 pinches the distributions along an axis in the $F_{\text{Pu}239} - F_{\text{Pu}}$ plane, according to the core content. This also has the effect of reducing the variance in the Gaussian distributions found in Fig. 3, which lowers the FPRs. Overall, Tab. II shows that this procedure reduces the FPR by at least a factor of 3 if the uranium-235 spectrum contains the bump and below $10^{-4}\%$ for a plutonium-239 bump. The FPR rates remain at or above $\sim 50\%$ for all removal scenarios across all measurement periods. The sensitivity to downgrading is also enhanced by the bump location. Less than 1% (20%) of the WGMOX (LEU+MOX) cores return plutonium fission grades above weapons at the last measurement period with a plutonium-239 bump.

This work has explored the abilities of a surface-deployed antineutrino detector to determine the core composition of the reactor it is monitoring via continuous spectral and rate measurements. The spectrum, with an interaction threshold of 2 MeV and binned into 250 keV bins, is fitted to an event distribution providing best-fit values for the fission rates of $^{235,238}\text{U}$ and $^{239,241}\text{Pu}$. These best-fit fission rates are combined into various fractions and we determine that for 500 d of ir-

radiation in a LWR, which will downgrade a full WGMOX core to RGMOX, we can establish this average downgrade with 84% confidence based on antineutrino monitoring. For a one-third WGMOX two-thirds LEU core we can determine the average downgrade with 69% confidence. Multiple measurement periods of 90 d within the irradiation cycle can differentiate between our four major core compositions with 95% accuracy. This is done mostly by comparing the plutonium-239 fission fraction, but can be reinforced with other fission fractions as well. Detecting the removal of plutonium from a mixed LEU and WGMOX core with an antineutrino detector is found to be incredibly difficult and highly reliant on the first measurement period. The existence of a spectral distortion in either the uranium-235 or plutonium-239 antineutrino fluxes only enhances the monitoring capabilities mentioned above, except for the detection of an intentional removal of plutonium.

We would like to acknowledge A. Bernstein, N. Bowden and A. Erickson for useful discussions and comments on an earlier version of this manuscript. This work was supported by the U.S. Department of Energy National Nuclear Security Administration under award DE-AC52-07NA27344 via sub-award B612358 from Lawrence Livermore National Laboratory.

* corresponding author: pjaffke@vt.edu

- [1] National Academy of Sciences, *Management and Disposition of Excess Weapons Plutonium* (The National Academies Press, 1994).
- [2] F. von Hippel and G. MacKerron (2015).
- [3] A. Borovoi and L. Mikaelyan, Soviet Atomic Energy **44**, 589 (1978), ISSN 0038-531X, URL <http://dx.doi.org/10.1007/BF01117861>.
- [4] A. Bernstein, Y.-f. Wang, G. Gratta, and T. West, J. Appl. Phys. **91**, 4672 (2002), nucl-ex/0108001.

- [5] A. Bernstein, N. S. Bowden, A. Misner, and T. Palmer, *J. Appl. Phys.* **103**, 074905 (2008), URL <http://scitation.aip.org/content/aip/journal/jap/103/7/10.1063/1.2899178>.
- [6] E. Christensen, P. Huber, and P. Jaffke, *Science and Global Security* **23**, 20 (2015), 1312.1959.
- [7] K. M. Heeger, B. R. Littlejohn, H. P. Mumm, and M. N. Tobin, *Phys. Rev.* **D87**, 073008 (2013), 1212.2182.
- [8] S. Oguri, Y. Kuroda, Y. Kato, R. Nakata, Y. Inoue, C. Ito, and M. Minowa, *Nucl. Instrum. Meth.* **A757**, 33 (2014), 1404.7309.
- [9] G. Boireau et al. (NUCIFER), *Phys. Rev.* **D93**, 112006 (2016), 1509.05610.
- [10] E. Christensen, P. Huber, P. Jaffke, and T. E. Shea, *Phys. Rev. Lett.* **113**, 042503 (2014).
- [11] N. S. Bowden, K. M. Heeger, P. Huber, C. Mariani, and R. B. Vogelaar (2016), 1602.04759.
- [12] P. Vogel and J. F. Beacom, *Phys. Rev.* **D60**, 053003 (1999), hep-ph/9903554.
- [13] P. Huber, *Phys. Rev.* **C84**, 024617 (2011), 1106.0687.
- [14] T. A. Mueller et al., *Phys. Rev. C* **83**, 054615 (2011), 1101.2663.
- [15] F. P. An et al. (Daya Bay), *Phys. Rev. Lett.* **116**, 061801 (2016), 1508.04233.
- [16] J. H. Choi et al. (RENO), *Phys. Rev. Lett.* **116**, 211801 (2016), 1511.05849.
- [17] J. I. Crespo-Anadón (Double Chooz), *Nucl. Part. Phys. Proc.* **265-266**, 99 (2015), 1412.3698.
- [18] J. Ashenfelter et al. (PROSPECT), *J. Phys.* **G43**, 113001 (2016), 1512.02202.
- [19] F. P. An et al. (Daya Bay) (2016), 1610.04802.
- [20] A. Erickson, A. Bernstein, and N. Bowden (2016), 1612.00540.
- [21] Carlson, J. and Bardsley, J. and Bragin, V. and Hill, J., in *IAEA Symposium on International Safeguards. Extended synopses* (1999).
- [22] N. M. Abdurrahman, R. C. Block, D. R. Harris, R. E. Slovacek, Y.-D. Lee, and F. Rodriguez-Vera, *Nuclear science and engineering* **115**, 279 (1993).
- [23] A. C. Hayes, J. L. Friar, G. T. Garvey, D. Ibeling, G. Jungman, T. Kawano, and R. W. Mills, *Phys. Rev.* **D92**, 033015 (2015), 1506.00583.
- [24] P. Huber, *Nucl. Phys.* **B908**, 268 (2016), 1602.01499.
- [25] A. C. Hayes and P. Vogel (2016), 1605.02047.